Optical feedback cooling of a mechanical silicon oscillator with a single laser

Master's thesis

Author:
Joonas Nätkinniemi

Supervisor:
Juha Muhonen

July 28, 2020

Department of Physics
University of Jyväskylä

Abstract

Nätkinniemi, Joonas
Optical feedback cooling of a mechanical silicon oscillator with a single laser
Master's thesis
Department of Physics, University of Jyväskylä, 2020, 51 pages

Optical feedback cooling was attempted on a split silicon beam photonic crystal oscillator, which acts as an optical cavity and a micromechanical resonator. The cooling setup uses a single laser for the dual roles of position measurement and feedback via amplitude modulation. The theoretical basis of optomechanical feedback cooling is explored, and expected spectrum of the feedback experiment is simulated. Feedback experiments were performed and the resulting spectrums were plotted and analyzed. Because of mistakes made in the experiment setup, significant unwanted parasitic feedback effect was encountered during the feedback experiments, which resulted in no detectable cooling effect. The probable significant causes of the parasitic feedback were identified and ways to correct them proposed for possible follow up experiments.

Keywords: thesis, abstract

Tiivistelmä

Nätkinniemi, Joonas
Mekaanisen piivärähtelijän optinen takaisinsyöttöjäähdytys yhdellä laserilla
Pro gradu -tutkielma
Fysiikan laitos, Jyväskylän yliopisto, 2020, 51 sivua

Optisella takaisinsyöttöjäähdytyksellä tarkoitetaan laserjäähdytyksen tyyppiä, jossa mekaanisen värähtelijän liike syötetään takaisin moduloimalla laserin amplitudia siten, että laserin amplitudi, ja täten säteilypaine, on suurimmillaan silloin kuin värähtelijän nopeus laseria kohti on suurimmillaan. Laserin säteilypaine vaimentaa värähtelijän lämpöliikkeestä johtuvaa värähtelyä, joka tarkoittaa sitä, että värähtelijän lämpötila laskee. Tässä työssä optista takaisinsyöttöjäähdytystä sovellettiin halkaistun piipalkki valohilan jäähdyttämiseen. Halkaistu piipalkki toimii optisena kaviteettina, muodostaen optomekaanisen systeemin. Värähtelijän liikkeen mittaus ja liikkeen takaisinsyöttö suoritettiin yhtäaikaisesti samalla laserilla. Työssä myös käydään läpi optomekaniikan ja takaisinsyöttöjäähdytyksen teoriaa, sekä simuloidaan jäähdytyskokeen odotettu värähtelyspektri.

Jäähdytyskoetta suoritettaessa törmättiin ongelmiin parasiittisen takaisinsyötön kanssa. Näiden ongelmien johdosta minkäänlaista jäähtymistä ei saavutettu. Näistä jäähdytyskokeista mitatut spektrit piirrettiin ja analysoitiin. Kohdatut ongelmat parasiittisen takaisinsyötön kanssa johtuivat mittauksen valmistelussa tehdyistä virheistä. Värähtelijän liikkeen mittaamiseksi käytetyn homodyyni-interferometrin referenssi- ja signaalihaarojen välillä tulee olla tietty vaihe-ero. Tätä vaihe-eroa ei oltu asetettu oikein. Tämän lisäksi parasiittista takaisinsyöttöä lisäsi se, että laserin amplitudia moduloitiin jo ennen kuin lasersäde erotettiin homodyyni-interferometrin kahteen haaraan, sen sijaan että modulointi olisi suoritettu vain signaalihaarassa. Kolmanneksi, laserin aallonpituus säädettiin käsin optisen kaviteetin resonanssiin, sen sijaan että se olisi lukittu siihen sähköisesti. Tämä aiheutti pienen epävireen laserin ja optisen kaviteetin välille. Kunhan nämä virheet korjataan, pitäisi takaisinsyöttöjäähdytyksen jatkossa onnistua.

Avainsanat: opinnäyte, tiivistelmä

1 Introduction

Optomechanics is the field of study and application of interaction between light and mechanical motion. The basis of optomechanics is that light applies a radiation pressure force to a mechanical system, for example a suspended mirror, which then changes the motion of the system. The light reflected back from the system can also be used to gain information about the mechanical state of the system, such as information about the position of an oscillator. The action of light on mechanics has many applications, one of which is laser cooling.

The idea of using a laser to cool down matter was first proposed by Hänsch and Swallow[1], as well as Wineland and Dehmelt, both in 1975. Wineland then went on to conduct the first laser cooling experiment in 1978[2]. This first type, and still the most common type, of laser cooling is now known as Doppler cooling. In doppler cooling, the laser is slightly red detuned from the atoms electronic absorption wavelength. When the atom is moving towards the laser, the photon wavelength gets doppler shifted into the electronic absorption range and the photon is absorbed, slowing the atoms momentum. The atom then emits a photon in a random direction as it relaxes back to its electronic ground state. This process has an overall dampening effect on the atoms movement, thus cooling them down. Other types of laser cooling entered the picture in the following decades, such as Sisyphus cooling, resolved- and Raman sideband cooling, grey molasses, and cavity assisted cooling. These techniques are all related to doppler cooling, and work mostly for atoms or ions in a vacuum or in a trap, rather than macroscopic mechanical structures.

Optomechanical cooling first appeared in 1970, when Braginsky et al.[3] demostrated damping of mechanical motion due to radiation pressure on a microwave cavity. The first optomechanical experiment to use optical cavities was in 1983, by Dorsel et al.[4]. The first optomechanical experiment to demonstrate cooling was a 1999 experiment by Cohadon, Heidmann and Pinard[5], where they used optical feedback to cool a suspended mirror. This type of optomechanical cooling by active feedback, aka. feedback cooling or "cold damping", was first proposed the year before by Mancini et al,[6] and has since been used to cool, amongst other things,

AFM cantilevers[7], neutral atoms[8], nanoparticles, and various micro- and nanomechanical oscillators. Ground state cooling by feedback of a mechanical oscillator was first achieved by Rossi et al.[9] in 2018.

Feedback cooling works by reading the position of the mechanical oscillation, and then using it to create a feedback signal for modulating the amplitude of the cooling laser, so that the radiation pressure is proportional to the velocity of the oscillation, creating a strong damping force. The required measurement of the oscillator position is often done using a separate laser, tuned to different optical cavity mode (and different in polarization) to avoid interaction with the cooling laser. The effectiveness of feedback cooling depends, among other things, on the efficiency of the measurement of the oscillator position, with groundstate cooling requiring a high efficiency[9]. The measurement efficiency quantifies the amount of information gained per decoherence caused by the measurement. Since decoherence leads to heating, this efficiency should be as high as possible for best cooling performance.

The theoretical basis for feedback control of optical cavities was first explored by Wiseman and Wilburn in 1993[10]. The theoretical basis for feedback cooling was further refined, amongst others, in a 1999 paper by Doherty and Jacobs[11], where they establish a connection with classical control theory, allowing the theory of classical feedback loops to be applied to quantum systems. A more recent, comprehensive look on quantum control theory can be found in, for example, a 2017 paper by Zhang et al.[12]

Beside feedback cooling, there is another common optomechanical cooling method called sideband cooling. In sideband cooling, the cooling laser beam is red detuned from the optical cavity resonance, which results in an overall dampening force on the oscillation. This is closely analogous with the way doppler cooling works. Sideband cooling acts passively, as opposed to the active feedback in feedback cooling, and works best in the resolved sideband regime of optical cavities. Passive cooling by photothermal force was first demonstrated by Metzer et. al.[13] in 2004, by cooling a microlever from room temperature down to 18K. Passive cooling based on radiation pressure induced backaction force, which is what is commonly understood as sideband cooling, was first demonstrated on a micromechanical oscillator in 2006 by both Arcizet et al.[14] and Schliesser et al.[15] Sideband cooling has been used to get mechanical systems to their groundstate, with lowest phonon occupation of $\bar{n} \approx 0.2$ achieved by Peterson et al.[16] in 2016. This type of cooling is typically limited by the quantum back-action limit, where the cooling is limited by the heating caused by the back-action

of the radiation pressure shot noise[17][18]. There are ways around this limit while still using a passive sideband cooling method, but by contrast, feedback cooling is not usually primarily limited by shot noise, being instead mainly limited by the instability at high feedback gains. The two methods of optomechanical cooling have been compared in a 2008 paper by Genes et al.[19], where the advantage of the active feedback cooling paradigm in the so-called bad-cavity limit is established.

In this work feedback cooling will be used on a split silicon beam, patterned with a photonic crystal, using a single laser. The split silicon beam structure, which is the same kind of structure as in the paper by Leijssen et al.[20], will be used in the future to study the coupling of donor spin qubits in silicon to the mechanical motion of the beam. For coherent coupling, the beam should be as cold as possible, which is why feedback cooling is being investigated. Feedback cooling has been shown to work well in the bad-cavity limit[19] where our cavity resides, and since a laser will be used to read the mechanical motion of the beam for the study of spin qubits, using the same laser to cool down the mechanical motion seems optimal. The reasoning for using a single laser for both measuring the mechanical motion and for applying the feedback force, instead of two seperate lasers as was done by Rossi et al.[9], was because there was only one suitable laser available at the time. This work will show that naively applying the feedback in this manner can lead to problems with parasitic self-feedback due to unwanted interaction of the balanced homodyne measurement setup with amplitude modulation of the measuring laser.

2 Theory

2.1 Harmonic oscillator

Like many physical systems, optomechanical systems can be modelled as coupled quantum harmonic oscillators, where both the mechanical oscillator and the cavity optical field are modelled as simple harmonic oscillators, connected to an outside thermal bath[18]. Quantum harmonic oscillators have a Hamiltonian of the form

$$\hat{H} = \frac{k\hat{q}^2}{2} + \frac{\hat{p}^2}{2m},$$

where m is the oscillator's mass, k is the spring constant and $\hat{q}$ and $\hat{p}$ are the position and momentum operators. The oscillator can also be described in terms of annihilation and creation operators a and $a^\dagger$, which act on the oscillator states to either add or remove a quantum (a phonon, or a photon in case of the optical field), moving the oscillator away or towards the ground state:

$$a|n\rangle = \sqrt{n}|n-1\rangle$$

$$a^\dagger|n\rangle = \sqrt{n+1}|n+1\rangle,$$

where $|n\rangle$ is the n:th eigenstate of the harmonic oscillator[18]. These operators are also called the ladder operators, because they have the effect of moving up or down an energy level, adding or removing a quantum of energy. Phonon/photon number operator $\hat{n}|n\rangle = n|n\rangle$ can be defined using the ladder operators as

$$\hat{n} \equiv a^\dagger a.$$

According to quantum mechanics, all mechanical systems have some energy even in ground state, called zero-point energy. Therefore, the oscillator also has some zero-point momentum p_{zp}, as well as some average zero-point displacement x_{zp}. These are given by

$$p_{zp} = \sqrt{\frac{\hbar m \Omega_0}{2}}$$

and

$$x_{zp} = \sqrt{\frac{\hbar}{2m\Omega_0}},$$

where Ω_0 is the resonance frequency of the oscillator[18]. For the sake of simplicity, all harmonic oscillators (both mechanical and optical) are assumed to have only one resonance mode here. With the help of the zero-point quantities, the quantum mechanical position and momentum operators can be expressed in terms of the creation and annihilation operators as follows:

$$\hat{q} = x_{zp}(a^\dagger + a)$$

and

$$\hat{p} = ip_{zp}(a^\dagger - a).$$

We can then express the harmonic oscillator Hamiltonian in terms of the creation and annihilation operators, getting

$$\hat{H} = \hbar\Omega_0 \left(a^\dagger a + \frac{1}{2}\right) = \hbar\Omega_0 \left(\hat{n} + \frac{1}{2}\right).$$

This form of the Hamiltonian is called the canonical quantum harmonic oscillator Hamiltonian[18]. In practice, the zero point energy term $\frac{\hbar\Omega_0}{2}$ is often left out when it is not important.

It is often useful to define dimensionless position and momentum operators

$$\hat{Q} = \frac{1}{\sqrt{2}}\frac{\hat{q}}{x_{zp}} = \frac{1}{\sqrt{2}}(a^\dagger + a)$$

$$\hat{P} = \frac{1}{\sqrt{2}}\frac{\hat{p}}{p_{zp}} = \frac{i}{\sqrt{2}}(a^\dagger - a)$$

where the position and momentum operators $\hat{q}$ and $\hat{p}$ have been expressed using the ladder operators, as well as zero-point displacement and momentum.

Another useful quantity to define is the susceptibility

$$\chi \equiv \frac{1}{m(\Omega_0^2 - \Omega^2 - i\Omega\gamma)},$$

where m is the effective mass of the oscillator, Ω is frequency, and γ is the frequency dependent dissipation[17]. Susceptibility quantifies the oscillator's frequency dependent response to outside force, peaking at the resonance frequency of the oscillator. In other words, in the frequency

domain we have $x(\Omega) = \chi F(\Omega)$, where $x(\Omega)$ and $F(\Omega)$ are the fourier transforms of the oscillator displacement and the displacing force, respectively. As seen later, optical force from a laser acts to modify the mechanical oscillators susceptibility, changing its response to thermal forces. Thus susceptibility is an important concept to understand in feedback cooling.

In quantum optomechanics, it is often useful to transition to a rotating frame of reference, to simplify some of the calculations. In such a frame, there are the dimensionless quadrature operators

$$\hat{X}(t) = \frac{1}{\sqrt{2}}(a^\dagger e^{i\Omega_r t} + a e^{-i\Omega_r t})$$

and

$$\hat{Y}(t) = \frac{i}{\sqrt{2}}(a^\dagger e^{i\Omega_r t} - a e^{-i\Omega_r t}),$$

where Ω_r is the rotation frequency of the frame. These operators are often used for the optical field, where they are called the amplitude and phase quadratures, respectively. These quadratures are important in measuring the position of the oscillator, because (in the case of zero detuning) the mechanical position information gets imprinted on the phase quadrature of the scattered light[18]. Thus, for the measured signal to be linearly proportional to the oscillator position, the measurement must be constructed in such a way that only the phase quadrature of the scattered optical field is measured.

2.2 Mechanical oscillator in thermal bath

A harmonic oscillator connected to a thermal bath has a Hamiltonian of the form

$$\hat{H} = \hat{H}_0 + \hat{V} = \hbar\Omega_0 a^\dagger a + \hat{H}_{bath} + \hat{V},$$

where $\hat{V} = \hat{q}\hat{F}$ is a forcing term, describing the force $\hat{F}$ that the oscillator experiences due to coupling with the bath, and $\hat{H}_0 = \hbar\Omega_0 a^\dagger a + \hat{H}_{bath}$ is the bare system Hamiltonian, neglecting zero point energy[18]. H_{bath} is the Hamiltonian of the thermal bath, the form of which is not important in this case. This system of the oscillator and bath evolves in time, with the forcing causing upwards transitions in the oscillator energy levels.

The transition probability is

$$P_{n\to n+1} = \frac{x_{zp}^2(n+1)}{\hbar^2} t S_{FF}(-\Omega_0),$$

where t is time and S_{FF} is the power spectral density of the forcing term force $\hat{F}$[18]. Power spectral density of a quantum operator $\mathcal{O}$ in frequency space is given by

$$S_{\mathcal{O}\mathcal{O}}(\Omega) = \int_{-\infty}^{\infty} \mathrm{d}\tau \, e^{i\Omega\tau} \left\langle \hat{\mathcal{O}}^\dagger(t+\tau)\hat{\mathcal{O}}(t) \right\rangle_{t=0} = \int_{-\infty}^{\infty} \mathrm{d}\Omega' \, \left\langle \hat{\mathcal{O}}^\dagger(-\Omega)\hat{\mathcal{O}}(\Omega') \right\rangle .$$

Unlike its classical counterpart, the quantum power spectral density is not symmetrical, ie. $S_{\mathcal{O}\mathcal{O}}(\Omega) \neq S_{\mathcal{O}\mathcal{O}}(-\Omega)$. Many properties of optomechanical systems depend instead on the symmetrised power spectral density

$$\bar{S}_{\mathcal{O}\mathcal{O}}(\Omega_0) \equiv \frac{S_{\mathcal{O}\mathcal{O}}(\Omega_0) + S_{\mathcal{O}\mathcal{O}}(-\Omega_0)}{2}.$$

Power spectral density can be used to define the dissipation rate

$$\gamma = \frac{x_{zp}^2}{\hbar^2}(S_{FF}(\Omega_0) - S_{FF}(-\Omega_0))$$

of an oscillator coupled to a thermal bath. The symmetrised power spectral density can be alternatively expressed using this dissipation rate as

$$\bar{S}_{FF}(\Omega_0) = m\gamma\hbar\Omega_0(2\bar{n}+1).$$

This expression is called the quantum fluctuation-dissipation theorem[18]. The spectrum of an oscillator driven only by thermal forces should look something like figure 2.1.

For an oscillator in thermal equilibrium, the power spectral density can be used to define temperature

$$T = \frac{\hbar\Omega_0}{k_B}\left[\ln\left(\frac{S_{FF}(\Omega_0)}{S_{FF}(-\Omega_0)}\right)\right]^{-1}$$

and mean phonon occupancy

$$\bar{n} = \frac{S_{FF}(-\Omega_0)}{S_{FF}(\Omega_0) - S_{FF}(-\Omega_0)},$$

where S_{FF} is the power spectral density of a force exerted on the oscillator due to coupling with an external bath. This result relies on the so-called sideband asymmetry. Often in optomechanics experiments, however, because the oscillator is being heated or cooled by a laser, it is not in

Figure 2.1: Simulated thermal spectrum of a mechanical oscillator with resonance frequency of 8.5MHz and mechanical damping rate of 200Hz. The mechanical resonator is driven purely by stochastic thermal forces, here simulated at a temperature of 295K.

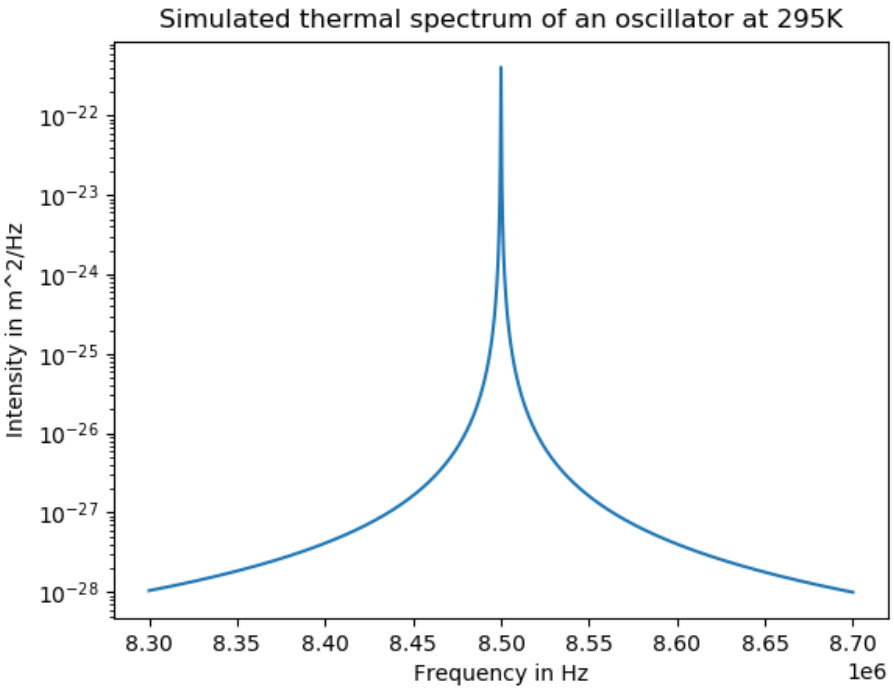

a thermal equilibrium. In such cases a frequency dependent effective temperature

$$T_{eff}(\Omega) = \frac{\hbar\Omega}{k_B}\left[\ln\left(\frac{S_{FF}(\Omega)}{S_{FF}(-\Omega)}\right)\right]^{-1}$$

can be defined[18].

The above equations for temperature rely on the sideband asymmetry of the thermal forcing force $\hat{F}$. However, the actual forcing force is rarely the thing that is measured. It is far more common to measure the oscillator position (using homodyne detection for example), and the equations for temperature and mean phonon occupancy can be derived similarly in terms of the oscillator position power spectral density sideband asymmetry:

$$T = \frac{\hbar\Omega_0}{k_B}\left[\ln\left(\frac{S_{QQ}(\Omega_0)}{S_{QQ}(-\Omega_0)}\right)\right]^{-1}$$
$$\bar{n} = \left(\frac{S_{QQ}(\Omega_0)}{S_{QQ}(-\Omega_0)} - 1\right)^{-1}.$$

These equations allow us, at least in theory, to calculate the temperature of a mechanical oscillator from its measured spectrum, giving us a way to measure the performance of our cooling system.

Using sideband asymmetry to measure temperature and phonon occupancy requires that the positive and negative components of the power spectral density are seperately measurable, which is not always the case. Relevant to this work, one such case is homodyne measurement of optical field phase, after its interaction with an oscillator[18]. In this case, the mean phonon occupancy (and from that the temperature) can be gleaned from the integral of the symmetrised power spectral density instead[18]:

$$\frac{1}{\pi}\int_0^\infty \mathrm{d}\Omega\, \bar{S}_{QQ}(\Omega) = \bar{n} + \frac{1}{2}.$$

For a system of a harmonic oscillator, coupled to a bath consisting of an ensemble of independent oscillators, a quantum Langevin equation

$$m\ddot{\hat{q}} + m\int_{-\infty}^{t} \mathrm{d}t'\, \gamma(t-t')\dot{\hat{q}}(t') + \frac{\partial\hat{V}(\hat{q})}{\partial\hat{q}} = \hat{F}(t)$$

can be defined, where $\hat{F}(t) = \sum_j k_j \hat{q}_j^h(t)$ is a stochastic force with zero expectation value, rising from interactions with the bath oscillators j.

Assuming linear damping of the form $\gamma(t) = \gamma\delta(t)$ is called the first Markov approximation, and results in a Markov Langevin equation of the form

$$m\ddot{\hat{q}} + m\gamma\dot{\hat{q}} + \frac{\partial\hat{V}(\hat{q})}{\partial\hat{q}} = \hat{F}(t).$$

This approximation is not strictly accurate for quantum systems, but is close enough to not matter in practice[18]. While in this work we only work with oscillator position $\hat{q}$, the Markov Langevin equation can also be generalised for any observable $\mathcal{O}$, becoming

$$\dot{\hat{\mathcal{O}}} = \frac{1}{i\hbar}\left[\hat{\mathcal{O}}, \hat{H}_{sys}\right] + i\sqrt{2\gamma}\left[\hat{\mathcal{O}}, \hat{Q}\right]\hat{P}_{in}(t) + \frac{1}{2iQ}\left\{\left[\hat{\mathcal{O}}, \hat{Q}\right], \dot{\hat{Q}}(t)\right\}_+,$$

where $\hat{H}_{sys} = \frac{\hat{p}^2}{2m} + \hat{V}(\hat{q})$, $Q = \Omega_0/\gamma$ is the quality factor of the oscillator, $\hat{P}_{in} \equiv \frac{x_{zp}\hat{F}(t)}{\hbar\sqrt{\gamma}}$ is the dimensionless input momentum fluctuation operator, and $\hat{Q}$ is the dimensionless position operator defined earlier[18]. Here the notation $\{\hat{A}, \hat{B}\}_+ = \hat{A}\hat{B} + \hat{B}\hat{A}$ denotes the anticommutator.

2.3 Cavity optomechanics

A Fabry-Pérot cavity with length L that has a one of the mirrors connected to a mechanical oscillator has optical modes with wavelength

$$\lambda_j = \frac{2(L-q)}{j},$$

where q is the mechanical displacement of the connected oscillator, and j is the mode number[18]. The corresponding mode frequencies of the cavity are given by

$$\Omega_{c,j}(q) = \frac{2\pi c}{\lambda_j} = \frac{\pi c j}{L-q},$$

where c is the speed of light. The shift of this frequency per displacement is the definition of optomechanical coupling strength

$$G \equiv \frac{\delta\Omega_{c,j}(q)}{\delta q} = \frac{\Omega_c}{L},$$

where Ω_c is the cavity frequency at zero displacement. A related important quantity is the vacuum optomechanical coupling rate

$$g_0 \equiv G x_{zp},$$

which quantifies the rate of frequency shift caused by displacement, in steps of zero-point motion. In other words, for every x_{zp} of displacement, the optical resonance frequency shifts by g_0. Another related quantity is the field-enhanced, or linearised, optomechanical coupling rate

$$g = g_0\sqrt{\bar{n}_{cav}},$$

where $\bar{n}_{cav}$ is the average photon number in the cavity[17].

The Hamiltonian of a typical optomechanical system (such as the one described above) is given by

$$\hat{H} = \hat{H}_M + \hat{H}_L = \frac{\hat{p}^2}{2m} + \frac{m\Omega_m^2}{2}\hat{q}^2 + \hbar\Omega_c(\hat{q})a^\dagger a,$$

where a and $a^\dagger$ are now annihilation and creation operators for the optical field, and Ω_m is the mechanical resonance frequency. This Hamiltonian can be expanded into

$$\hat{H} = \hbar\Omega_c a^\dagger a + \hbar\Omega_m b^\dagger b + \hbar g_0 a^\dagger a(b^\dagger + b),$$

where b and $b^\dagger$ are the annihilation and creation operators for the mechanical oscillator[18]. Usually in cavity optomechanics, the optical cavity resonance frequency Ω_c is much larger than the other frequencies in the system, which means it is convenient to move to a frame of reference rotating at the laser frequency Ω_L, removing fast oscillations of the optical field. The resulting Hamiltonian in the rotating frame is given by

$$\hat{H} = \hbar\Delta a^\dagger a + \hbar\Omega_m b^\dagger b + \hbar g_0 a^\dagger a(b^\dagger + b),$$

where $\Delta \equiv \Omega_c - \Omega_L$ is the detuning between the optical cavity and the laser frequency[18].

Coherent optical driving via a laser is common practice in optomechanics. This coherent driving force introduces an extra term into the Hamiltonian

$$\hat{H} = \hbar\Delta a^\dagger a + \hbar\Omega_m b^\dagger b + \hbar g_0 a^\dagger a(b^\dagger + b) + \hbar\epsilon(a^\dagger + a),$$

where ϵ is the drive strength. This optical driving introduces a steady-state displacement in both the position of the mechanical oscillator and the amplitude of the cavity field away from zero. It is then practical to displace the Hamiltonian by shifting the frame of reference such, that the displacements in the steady-state are zero. Thus displaced Hamiltonian has the form

$$\hat{H} = \hbar(\Delta - \frac{2g_0^2\alpha^2}{\Omega_m})a^\dagger a + \hbar\Omega_m b^\dagger b + \hbar g_0[\alpha(a^\dagger + a) + a^\dagger a](b^\dagger + b),$$

where $\alpha = -\frac{\epsilon}{\Delta+2\langle b\rangle g_0}$ is the displacement of the cavity field amplitude in the steady state[18]. This Hamiltonian can be linearised by dropping the term $a^\dagger a$ in the square brackets, on the grounds of it being negligible compared to the other terms because $\langle a\rangle = 0$ in the displaced frame[18]. In this linearised picture, the definition of optical detuning in usually changed to include the modification induced by the displacement, such that

$$\Delta \to \Delta + \frac{2g_0^2\alpha^2}{\Omega_m}.$$

Applying these changes to the Hamiltonian, it becomes

$$\begin{aligned}\hat{H} &= \hbar\Delta a^\dagger a + \hbar\Omega_m b^\dagger b + \hbar g(a^\dagger + a)(b^\dagger + b) \\ &= \frac{\hbar\Delta}{2}\left(\hat{X}^2 + \hat{Y}^2\right) + \frac{\hbar\Omega_m}{2}\left(\hat{Q}^2 + \hat{P}^2\right) + 2\hbar g\hat{X}\hat{Q},\end{aligned}$$

where we have replaced $g_0\alpha$ with g, because $|\alpha|^2 = \bar{n}_{cav}$. This Hamiltonian is the linearized cavity optomechanical Hamiltonian[18]. For most optomechanical systems, this linearised picture is accurate enough, but for some systems, such as this one[20], this approximation breaks down, and non-linear effects become significant.

For optomechanical systems, the optical and mechanical decoherence rates, $\kappa_{decoh} = \kappa$ and $\Gamma_{decoh} = \Gamma(2\bar{n}+1)$ are important parameters. These decoherence rates quantify the rate at which the optical and mechanical degrees of freedom decohere due to interaction with the environment. Due to the high frequency of optical systems resulting in low thermal occupancy ($\bar{n} \approx \frac{k_B T}{\hbar\Omega}$), the optical decoherence rate is roughly equal to the optical dissipation rate κ. The mechanical decoherence rate is, in addition to the mechanical dissipation rate Γ, also affected by the mean phonon occupancy $\bar{n}$[18].

When the location of a quantum mechanical object is observed, there is always certain amount of momentum uncertainty that is introduced to the system, as per the Heisenberg uncertainty principle. This increase in momentum uncertainty is called quantum back-action. This back-action is an important concept in optomechanics, due to its effects on the temperature of the resonator, and thus on the mean phonon occupancy $\bar{n}$[18].

Important metric for quantifying optomechanical systems, optomechanical cooperativity

$$C \equiv \frac{4g^2}{\kappa\Gamma}$$

measures the optomechanical coupling strength against the optical and mechanical dissipation rates. There is also the effective optomechanical cooperativity

$$C_{eff} \equiv \frac{C}{(1-2i\omega/\kappa)^2},$$

which, among other things, gives the optomechanical coupling strength necessary for the quantum mechanical back-action of the optical beam to heat the mechanical oscillator by one phonon[18].

Depending on the various optomechanical parameters introduced above, optomechanical systems can be divided into several regimes of interest. There is for example the strong-coupling regime of $g > \kappa,\Gamma$, where the optical mode driven by laser and the mechanical oscillation mode hybridize, and the harder to achieve single-photon strong-coupling regime $g_0 > \kappa,\Gamma$. Lots of interesting phenomena are expected to happen in the single-photon strong-coupling regime[17], such as visible nonlinear quantum effects[17]. With increasing g_0/κ, before the single-photon strong-coupling regime, there is the regime of $g_0\sqrt{2\bar{n}_{th}} \geq \kappa$, where this experiment operates. This regime is characterised by thermal motion inducing frequency fluctuations larger than optical linewidth[20], and exhibits nonlinear behaviour in all phenomena, relevantly including oscillator displacement measurements.

For cooling, the relevant regimes are the sideband-resolved regime of $\kappa \ll \Omega_m$, where sideband cooling is most effective, and the so-called bad-cavity limit of $\kappa \gg \Omega_m$, where feedback cooling is effective[19]. This experiment operates in the bad-cavity limit. A "bad cavity" means that sideband cooling to the groundstate is not possible[19], but also makes continuous measurement of the oscillator position practical, since the delay between light entering and exiting the cavity (ie. the inverse of optical decay rate κ) is so low compared to the oscillation period[11]. This continuos measurement is a requirement for the real-time feedback needed for optomechanical feedback cooling to be effective.

2.4 Homodyne interferometry

The physics of beam-splitters are central for understanding interferometry. For a beam splitter like in figure 2.2, the quantum mechanical treatment gives as outputs

$$\hat{a}_2 = r\hat{a}_1 + t'\hat{a}_0, \quad \hat{a}_3 = t\hat{a}_1 + r'\hat{a}_0,$$

Figure 2.2: Quantum mechanical beam-splitter

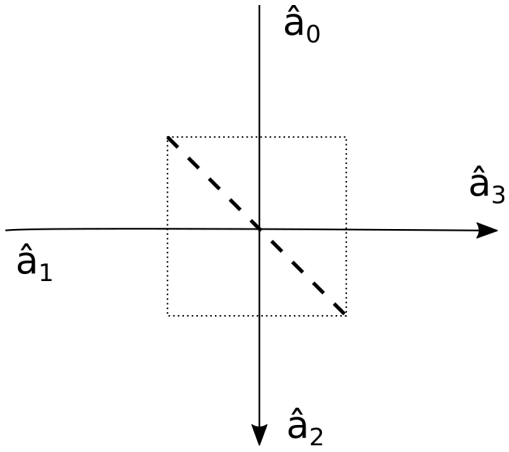

where $\hat{a}_0$ and $\hat{a}_1$ are the annihilation operators of the two input ports, $\hat{a}_2$ and $\hat{a}_3$ are the annihilation operators for the beamsplitter output ports, and t, t', r and r' are the complex transmittances and reflectances of the beam splitter. The operators for the input and output fields must satisfy the following commutation relations[21]:

$$\left[\hat{a}_i, \hat{a}_j^\dagger\right] = \delta_{ij}, \quad [\hat{a}_i, \hat{a}_j] = 0 = \left[\hat{a}_i^\dagger, \hat{a}_j^\dagger\right] \quad (i, j = 1, 2, 3).$$

These relations hold as long as

$$|r'| = |r|, \quad |t| = |t'|, \quad |r^2| + |t|^2 = 1, \quad r^* t' + r' t^* = 0, \quad r^* t + r' t'^* = 0$$

are true. This set of equations is known as the reciprocity relations. In the case of a 50/50 beam-splitter, this results in outputs

$$\hat{a}_2 = \frac{1}{\sqrt{2}}(\hat{a}_0 + i\hat{a}_1), \quad \hat{a}_3 = \frac{1}{\sqrt{2}}(i\hat{a}_0 + \hat{a}_1). \tag{2.1}$$

Notice the phase shift of $i = e^{i\pi/2}$ for the reflected waves. Also notice that both of the input ports must be taken into account, even if one of them consists only of the vacuum field.

If we take a coherent light wave with complex amplitude α, split it in a 50/50 beam-splitter into two arms of differing length (thus introducing a phase difference of θ), and recombine it again in a second 50/50 beam-splitter, then the outputs states of the second beam-splitter are given by

$$\left|\frac{i(e^{i\theta}+1)\alpha}{\sqrt{2}}\right\rangle \left|\frac{(e^{i\theta}-1)\alpha}{\sqrt{2}}\right\rangle.$$

If we then subtract the intensities of these two beams from each other, like in a balanced homodyne interferometer, we get[21] a final signal of

$$\langle \hat{O} \rangle = |\alpha|^2 \cos\theta.$$

In order to derive the final signal in of a balanced homodyne detector, with the signal branch a_S and local oscillator branch a_{LO}, we can use equation (2.1) and get

$$\hat{a}_+ = \frac{1}{\sqrt{2}}(\hat{a}_s + i\hat{a}_{LO}), \quad \hat{a}_- = \frac{1}{\sqrt{2}}(i\hat{a}_s + \hat{a}_{LO})$$

for the final beamsplitter output ports. Since a balanced homodyne detector works by substracting the signal of one port from the other, we then have the final homodyne signal strength as

$$H = \hat{a}_+^\dagger \hat{a}_+ - \hat{a}_-^\dagger \hat{a}_- = i(\hat{a}_s^\dagger \hat{a}_{LO} - \hat{a}_{LO}^\dagger \hat{a}_s). \tag{2.2}$$

To relate the signal branch annihilation operator $\hat{a}_s$ back to the mechanical movement of the cavity, we need to look at the input-output relations for the optical cavity. The output from the cavity ($\hat{a}_s$) relates to the field in the cavity by

$$\hat{a}_s = \sqrt{\kappa}_{out}\hat{a}, \tag{2.3}$$

where $\hat{a}$ is the intracavity field annihilation operator and κ_{out} is the cavity output dissipation rate. The intracavity field is given by

$$\hat{a} = \frac{\sqrt{\kappa}_{in}\hat{a}_{in}}{-i\Delta_c + \frac{\kappa}{2}},$$

where $\hat{a}_{in}$ is the cavity input field annihilation operator, cavity detuning $\Delta_c = \Delta + Gx$, Δ being the laser detuning from the cavity resonance and x being the mechanical displacement. The local oscillator arm gets a phase difference θ to the signal arm due to different path lengths, so we replace $\hat{a}_{LO}$ with $|\alpha_{LO}|e^{i\theta}$, where we have now moved from the annihilator operator depiction to complex amplitudes α. If we now input the above into equation (2.3), and that equation into equation (2.2), replacing $\hat{a}_{in}$ with $|\alpha_{in}|$ we get

$$H = |\alpha_{LO}|\frac{4\sqrt{\kappa_{in}\kappa_{out}}}{\kappa}\frac{|\alpha_{in}|}{1 + (\frac{2\Delta_c}{\kappa})^2}\left(\cos\theta + \frac{2\Delta_c}{\kappa}\sin\theta\right). \tag{2.4}$$

Since $(\frac{\Delta_c}{\kappa})^2 << 1$, assuming small Gx and large κ (as is usually the case in the bad cavity limit), we can see that with zero detuning Δ, so that

$\Delta_c = Gx$, the homodyne signal depends on the mechanical displacement x linearly when $\theta = \pi/2$, corresponding with measurement of the phase quadrature $\hat{Y}(t)$. Conversely, the signal does not depend on x at all when $\theta = 0$, corresponding to the measurement of the amplitude quadrature $\hat{X}(t)$. In addition, the signal also depends linearly on both the local oscillator field amplitude $|\alpha_{LO}| = \langle \hat{a}_{LO} \rangle$ and the cavity input field strength $|\alpha_{in}| = \langle \hat{a}_{in} \rangle$. We can also see that nonzero laser detuning can add considerable error to the position measurement.

The power spectral density of the detected homodyne photocurrent $\hat{i}$ is equal to the symmetrized power spectral density of the measured quadrature, i.e.

$$S_{\hat{i}\hat{i}}^{homo}(\Omega) = \bar{S}_{X_{det}^{\theta} X_{det}^{\theta}}(\Omega).$$

When the phase quadrature $\hat{Y} = \hat{X}_{det}^{\pi/2}$ is measured, this detected power spectral density also relates to the power spectral density of the mechanical oscillator position by

$$S_{\hat{i}\hat{i}}^{homo}(\Omega) = \frac{1}{2} + 4\eta\Gamma|C_{eff}|\bar{S}_{QQ}(\Omega),$$

where η is the detection efficiency, accounting for light lost to various scattering and absorption processes, and overall inefficiency of the detection[18].

2.5 Feedback cooling

Constant measurement of the oscillator position can be used to construct a feedback loop to cool the oscillator. The position data is first filtered to the frequency of a single mechanical oscillation mode, and then used to modulate the amplitude of a laser, such that the peak amplitude corresponds to peak velocity of the oscillation in the direction of the incoming laser beam. In other words, the amplitude of the laser is then proportional to the velocity of the oscillation. This causes a friction force, thus damping the oscillation[9]. Since the velocity of the oscillation is offset by $\pi/2$ in phase from its position (i.e. the velocity is the greatest when the displacement is zero), the phase of the feedback signal should be set to $-\pi/2$ relative to the measured oscillator displacement, while also accounting for the delay in the feedback loop. This type of feedback cooling is sometimes also called "cold damping"[17].

The oscillator position is measured using homodyne detection. As explained in the previous section, homodyne detection measures an arbitrary

Figure 2.3: Diagram of the feedback setup, according to classical control theory.

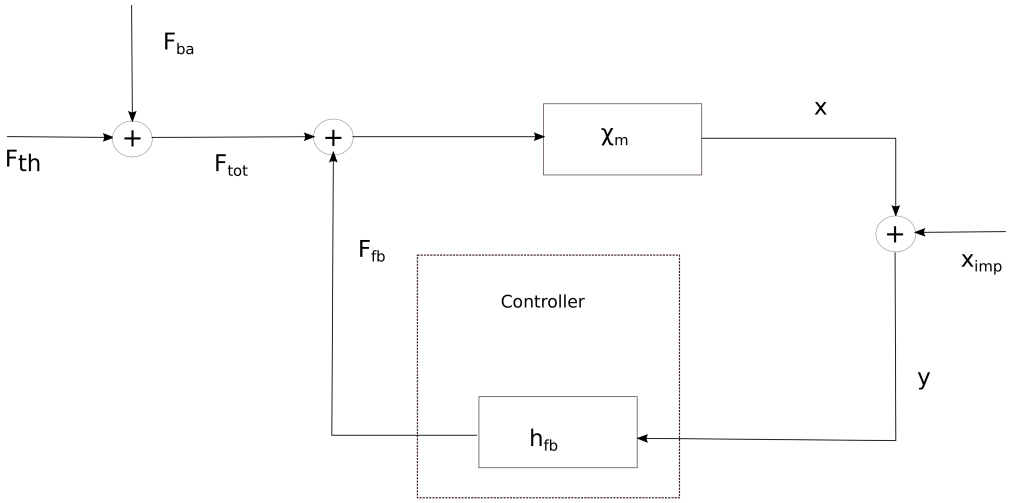

quadrature $\hat{X}^{\theta}_{det}$ of the detected optical field by interfering it with a bright local oscillator field of the same frequency. The measured quadrature in a homodyne setup depends on the phase difference of the local oscillator branch and the signal branch. The phase difference, in turn, depends on the relative path lengths of the two branches. To measure the correct quadrature, which in this case is the phase quadrature $\hat{Y}(t)$ of the optical field, the path length of the local oscillator arm must be adjusted, using for example a piezo mounted mirror. Since large amplitude fluctuations in the incoming light have an effect on the measurement outcome, as seen from equation (2.4), stabilizing the laser output power is a good idea.

From classical control theory, we can construct a diagram of the balanced homodyne measurement setup as in figure 2.3. From the diagram we get equations for detected oscillator position $y = x + x_{imp}$, the feedback force $F_{fb} = h_{fb}y$ and the actual oscillator position $x = \chi_m(F_{tot} + F_{fb})$. The position imprecision x_{imp} arises from optical shot noise. In the ideal case of zero detuning of the laser, this imprecision is uncorrelated with the backaction force[9]. In absence of feedback, the only forces acting on the oscillator are the stochastic thermal force F_{th}, and the quantum back-action force F_{ba}, which is caused by the coupling of the oscillator to the measurement laser.

From this group of equations, we can solve for the oscillator position x,

and find

$$x = \frac{\chi_m(\Omega)}{1 - \chi_m(\Omega)h_{fb}(\Omega)}(F_{tot} + h_{fb}(\Omega)x_{imp}) = \chi_{eff}(\Omega)(F_{tot} + h_{fb}(\Omega)x_{imp}),$$

where we have defined the effective susceptibility

$$\chi_{eff}(\Omega) = \frac{\chi_m(\Omega)}{1 - \chi_m(\Omega)h_{fb}(\Omega)},$$

where $h_{fb}(\Omega)$ is the transfer function of the feedback controller and $\chi_m(\Omega)$ is the mechanical susceptibility of the oscillator[9].

By rearranging the effective susceptibility equation to the form

$$\chi_{eff}(\Omega) = \frac{1}{\frac{1}{\chi_m(\Omega)} - h_{fb}(\Omega)} = \frac{1}{m\left(\Omega_m^2 - \Omega^2 - i\Gamma_m\Omega\right) - h_{fb}(\Omega)},$$

we can now see that the real part of the transfer function $h_{fb}(\Omega)$ has the effect of modifying the mechanical resonance frequency Ω_m, while the imaginary part of the transfer function modifies the mechanical damping rate Γ_m.

2.6 Signal processing

Bandpass filter is an electronic filter that lets only signals in a given frequency range through it, attenuating all other signals. Bandpass filters have a center frequency Ω_c, and a bandwidth Γ, which specifies the range of frequencies that pass the filter around the center frequency. In an analog circuit, a simple bandpass filter can be, for example, an RLC-circuit. However, analog filters have many drawbacks, making them impractical for some applications, such as a tendency for their charasteristics to drift with time and temperature.

In contrast, digital filters are more complex, but can be implemented in silicon using, for example, a programmable logic device, such as an FPGA (Field Programmable Gate Array)[22]. They can also be made very high order, and are programmable, which makes them easy to change on the fly. A drawback of the digital filter is, however, the introduction of some latency, as a result of the necessary analog-to-digital and digital-to-analog conversions.

An FPGA is a type of programmable logic circuit. The advantages of programmable logic circuits from a user standpoint, compared to the

Figure 2.4: Red Pitaya FPGA-board with its inputs and outputs. The board is connected to a computer via the Ethernet port. Picture taken from the official Red Pitaya documentation[23].

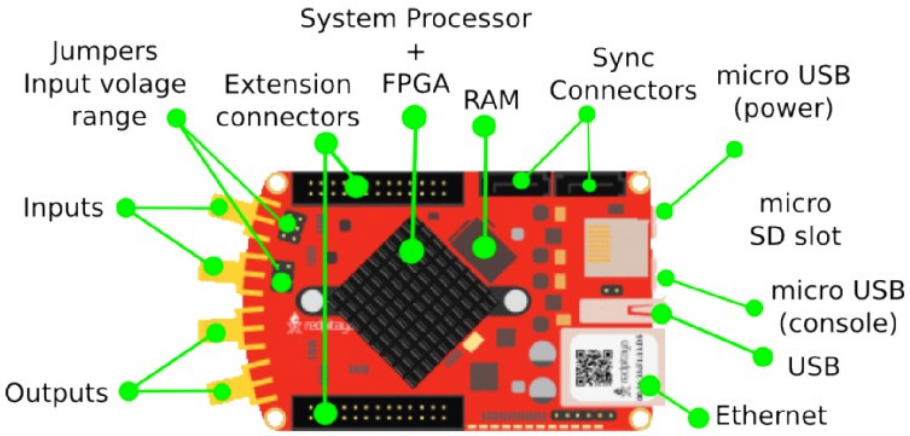

more common application specific integrated circuits (ASIC), is the ability to implement various custom specialized hardware into the silicon, using a hardware programming language such as VHDL or Verilog, based on the requirements of the specific task at hand. The same FPGA can then be reused later for a different task by simply reprogramming it. The disadvantages are usually a higher price for the same performance (compared to a comparable ASIC), and lower maximum general compute performance.

The Red Pitaya (aka. STEMlab) is an FPGA board that integrates two analog inputs and outputs[23], as can be seen in figure 2.4. The analog outputs have a maximum voltage range of ± 1V, which somewhat limits the amplitude of our feedback signal. The Red Pitaya board comes with a Xilinx Zynq 7010 FPGA, and with an SD-card that contains a chip design with some signal processing modules implemented, such as arbitrary signal generator, oscilloscope, PID modules, and three iq modules, implemented in Verilog HDL (Hardware Description Language). These iq modules can relevantly also be used as digital bandpass filters (up to 4th order) with adjustable gain and phase. Red Pitaya also integrates Python as a scripting language.

We use the pyrpl software package[24] to interface with the Red Pitaya. The pyrpl package has its own precompiled FPGA bitfile, which it uses to

implement the hardware for its various modules on the FPGA of the Red Pitaya. In principle, this hardware design can be customized by editing and compiling the Verilog source code into a new bitfile, but in this work the precompiled bitfile is used as-is.

In this work we use a fourth order band-pass filter, implemeted using the Red Pitaya iq module with pyrpl, with a transfer function of the form

$$h_{fb}(\Omega) = g_{fb} e^{i\Omega\tau - i\phi} \left[\frac{\Gamma_{fb}\Omega}{\Omega_{fb}^2 - \Omega^2 - i\Gamma_{fb}\Omega} \right]^2, \tag{2.5}$$

where g_{fb} is the total controller gain from all sources, including the adjustable electronic gain from Red Pitaya, as well various transduction factors. τ is the total controller loop delay, ϕ is the electronically set phase for the Red Pitaya's Lorentzian filter, Γ_{fb} is the filter bandwidth and Ω_{fb} is the filter center frequency. Looking closer at the equation, it consists of the gain constant g_{fb}, the phase factor $e^{i\Omega\tau - i\phi}$, which takes into account the loop delay time τ, consisting of electronic delay, as well as the delay caused by the finite speed of light of the laser beam's propagation through the homodyne setup, as well as the adjustable phase ϕ. The term inside the square brackets is the actual form of the bandpass filter, as built into the Red Pitaya iq module, itself a combination of a basic highpass and a lowpass filter. A basic bandpass filter is a second order filter, and by adding two of them in a series (hence the rise to the second power), you get a fourth order filter. The "order" of a filter refers to the highest power of the Ω term in its transfer function.

The Red Pitaya is here only used to create the feedback signal, but it can potentially be used for other relevant tasks, such as using the PID modules for creating a feedback loop locking the laser wavelength to the optical cavity resonance, or using the internal spectrum analyzer to monitor the signal[24].

3 Experiments and simulations

3.1 Measurement setup

The measurement setup consists of the Toptica CTL variable wavelength laser with wavelength range of 1460-1570nm, the sample in a cryostat, the Electro Optic Modulator (EOM), beamsplitters, mirrors, and photodetectors. These elements are arranged into the two arms of the balanced homodyne interferometer as in figure 3.1. The EOM is connected to the laser source by optical fiber, and after the EOM, the laser propagates in free space through the rest of the homodyne interferometer. The piezo mirror in the local oscillator arm is set to sweep, as in [20], and not fixed to the correct position for measurement of the phase quadrature like it should be for feedback, by mistake. The optical intensity in the signal arm is reduced by the use of a filter, before reaching the sample. As was discussed in the theory section, the homodyne signal of equation (2.4) is proportional to the oscillator displacement as long as the local oscillator path length is set correctly, so that the correct cavity output quadrature is measured.

After measurement, the measured photocurrent data is sent to a spectrum analyzer and to the Red Pitaya. The Red Pitaya, in combination with the pyrpl software package[24], is used to create the feedback signal by applying a fourth order bandpass filter with adjustable phase and gain to the input photocurrent data (see equation (2.5)), the output of which is sent to the EOM. The EOM modulates the laser amplitude in proportion to its control voltage, and since the control voltage here is filtered to be proportional to the oscillator velocity, so is the laser amplitude. The separate spectrum analyzer is used to record the photodiode output data in frequency domain, which is then plotted with python.

The feedback measurements are taken by first manually adjusting the laser wavelength to the cavity resonance and setting the bandpass filter center frequency Ω_{fb} in equation (2.5) equal to Ω_m of the mechanical mode that we are cooling, and then using a python script to adjust the phase of the feedback in steps from $-\pi$ to π, while measuring the spectrum at each step. The intention is to empirically find the controller phase where the

Figure 3.1: The basic measurement setup layout. Notice especially the EOM before the beamsplitter that splits into the LO- and signal arm.

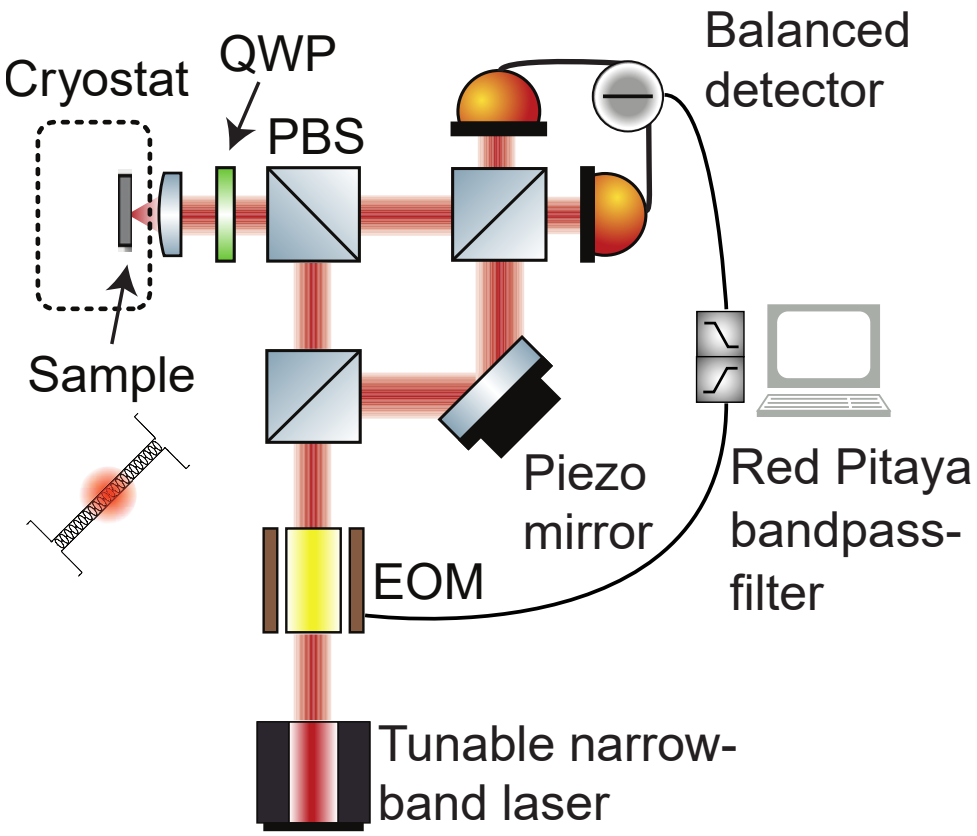

Figure 3.2: Simulation of the expected effect of the feedback on the spectrum. Notice the change in the damping of the oscillation. The simulation here is only for a single mechanical mode, and does not reflect the reality of the two mechanical modes we see in practice.

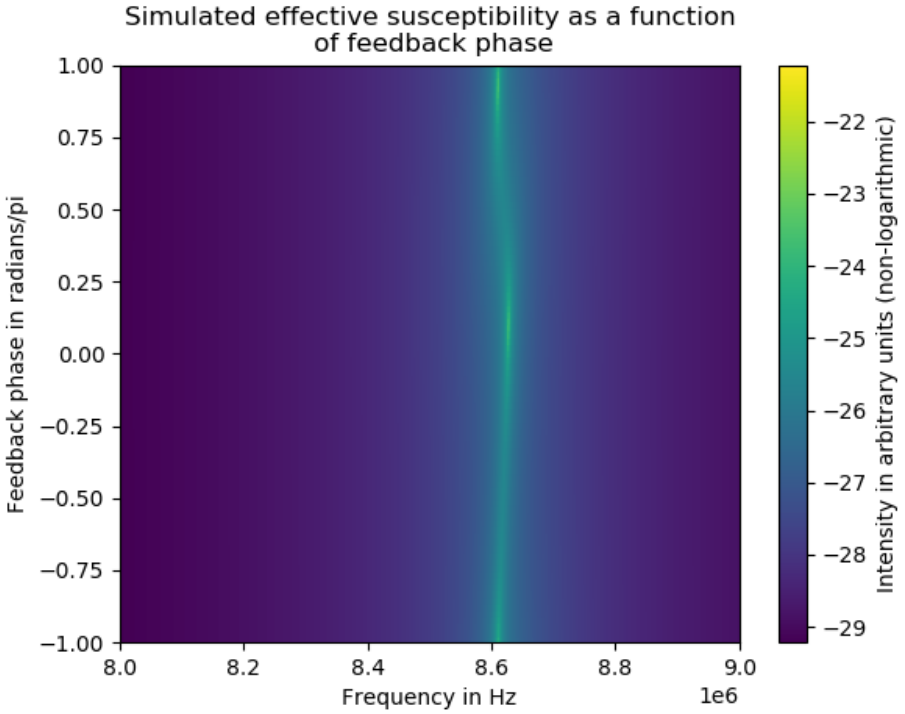

feedback is $-\pi/2$ behind the mechanical oscillation (see chapter 2.4), and a suitably high gain where the cooling effect is noticable in the measured spectrum. The data is plotted as a spectrograph for different controller gains, with frequency on the x-axis and controller phase on the y-axis. The measured feedback spectrum should look something like figure 3.2 as a function of controller phase for an effective gain, where the mechanical oscillation gets dampened with some phase and amplified with another.

3.2 Power stabilization

The laser power of the Toptica CTL laser has a tendency to wander when the laser is used in scan mode. To counteract this, we used the power

stabilization function provided by the Toptica DLC Pro laser controller. A 70/30 beam splitter was used to fork the laser to an external photodiode, which was used to read the laser power for the feedback loop. The power reading from the external photodiode was calibrated to roughly match the internal power reading of the CTL laser head in steady state.

Toptica DLC Pro provides the possibility of using the CTL internal photodiode power reading for the power stabilization feedback, which is useful for accounting for the internal losses and power changes due to changing laser wavelength, but does not account for losses in the outgoing fiber. Adding the EOM after the laser significantly increased the losses in the fiber, due to incompatible fiber connection types (angle polished connection of the laser vs straight fiber connection of the EOM). This made the power of the beam exiting the fiber after the EOM rather unstable, and made power stabilization via external photodiode rather appealing.

The external photodiode was a Thorlabs S122C standard photodiode, connected to a Thorlabs PM100D power meter. The power meter reading was fed via the 0-2V analog output to the "Fine-1" analog input of the DLC Pro controller, and used to feed its internal PID controller controlling the power stabilization. Since the output voltage of the power meter changes depending on the selected measurement range, it is important to keep the same range throughout. Changing the range requires recalibrating the power stabilization system.

3.3 Feedback via laser amplitude modulation

The feedback setup is shown in fig3.3, and consists of the balanced homodyne detector (Thorlabs PDB465C), Red Pitaya (aka. STEMlab) FPGA board that is used to generate the feedback signal, and an electro-optic modulator (EOM) that is used to modulate the amplitude of the laser based on the feedback signal. A significant problem with this setup is that the periodic amplitude modulation shows as a strong signal on the detector. This means that using a naive feedback scheme of merely feeding back the bandpass filtered signal means the feedback signal will be added on top of the actual signal, leading to the feedback force growing without bound until it saturates the Red Pitayas output, as can be seen in figure 3.4. The same effect happens even when the bandpass filter is placed outside of the mechanical modes, as can be seen in figure 3.5. If the gain is small enough where this does not noticably happen, then nothing happens, and no measurable cooling is happening.

Figure 3.3: Diagram of the feedback setup. The unwanted parasitic feedback z is added to to the oscillator position and its measurement imprecision to form the measured position signal y.

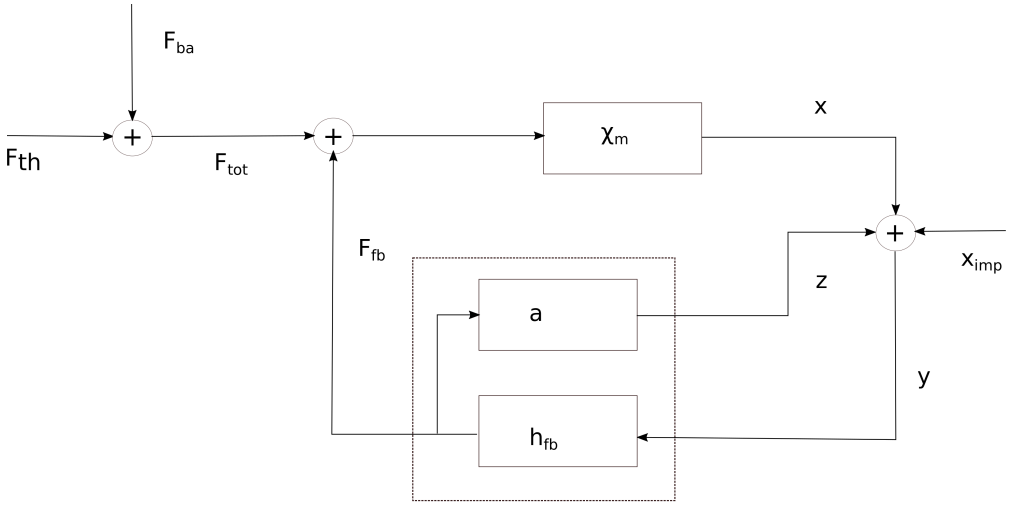

This unwanted positive feedback loop is modeled by adding another feedback path straight from the controller output to its input, going through some process a that has its own gain (including transduction factors) g_a and adds some delay τ_a:

$$a = g_a e^{i\Omega\tau_a}.$$

The unwanted feedback has the effect of modifying the effective susceptibility, which will interfere with the feedback. Comparing the effective susceptibilities in the ideal case of no unwanted feedback, i.e effective feedback in fig 3.6, and with the unwanted feedback in fig 3.7, we can see the effect.

Without the parasitic feedback, the detected oscillator position $y = x+x_{imp}$ is a sum of the actual position x and some measurement imprecision x_{imp}. Adding the self-feedback, we get an additional term for the detected oscillator position from the direct effect of the amplitude modulation, so that detected "oscillator position" is now

$$y = x + x_{imp} + z,$$

where $z = ah_{fb}y$ is the effect of the amplitude modulation on the detector. Of course now y no longer really corresponds to the oscillator position in any real way, which is the source for all the trouble here. Plugging in z to

Figure 3.4: Practical effect of unwanted feedback on the homodyne detection. Here we can see the phase response for the parasitic feedback, as well as severe artifacting, resulting mainly from the saturation of the Red Pitaya controller output. The electronic gain on the Red Pitaya is 1.4, while the filter bandwidth is 77kHz

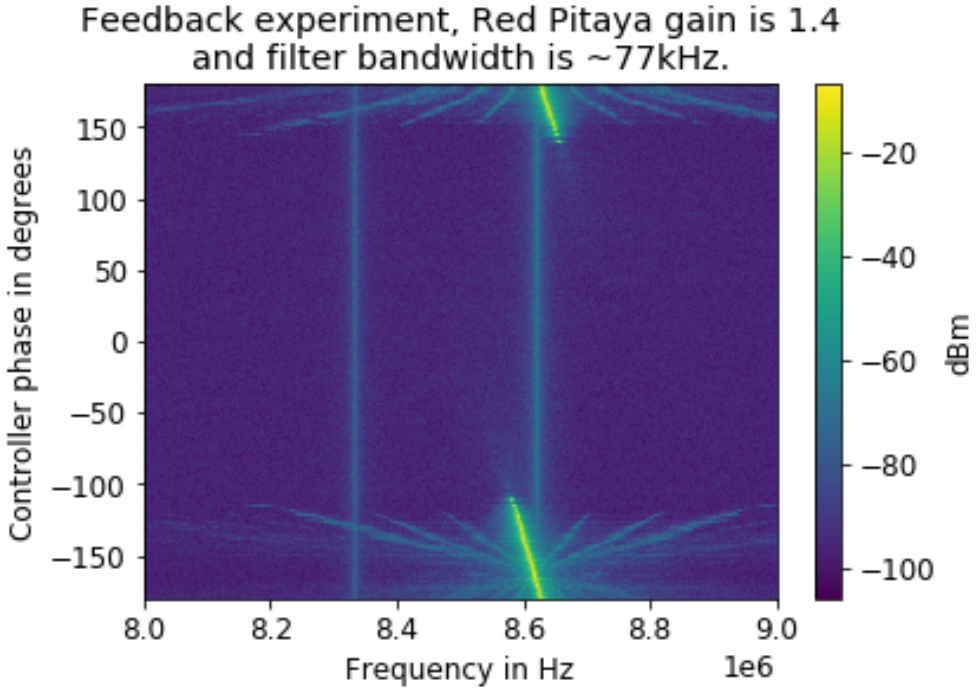

Figure 3.5: Practical effect of unwanted feedback on the homodyne detection. Here we can see the same artifacting and phase response, even when the filter is not on the mechanical mode. The electronic gain on the Red Pitaya is 1.5, while the filter bandwidth is 77kHz

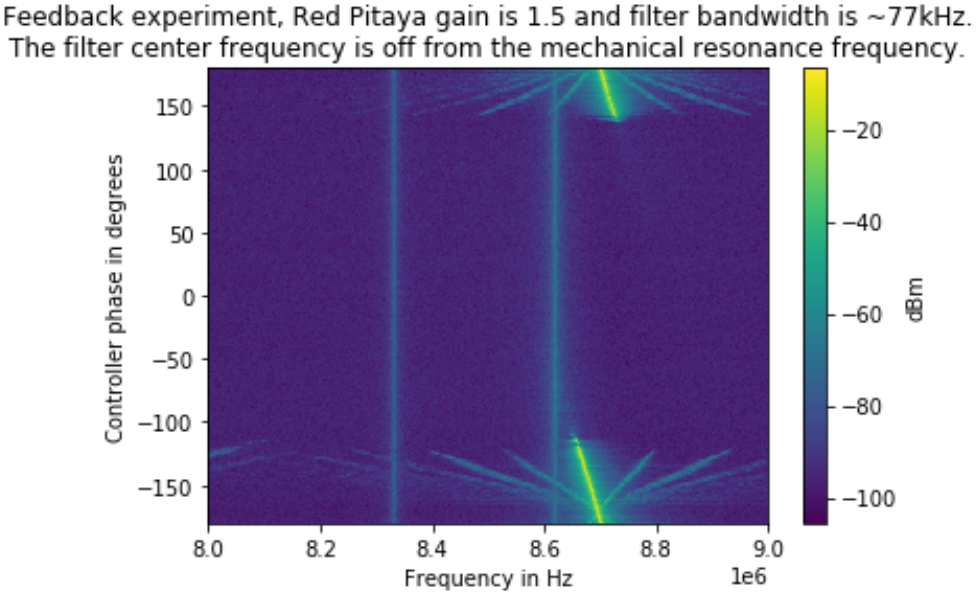

Figure 3.6: Simulated effective susceptibility vs. mechanical susceptibility without feedback. In the absence of the unwanted parasitic feedback, we can see the wanted effect of the feedback on the effective susceptibility when the feedback phase is exactly $-\pi/2$ behind the mechanical phase, with a simulated total gain of $7 * 10^{12}\text{kg} * \text{Hz}^2$.

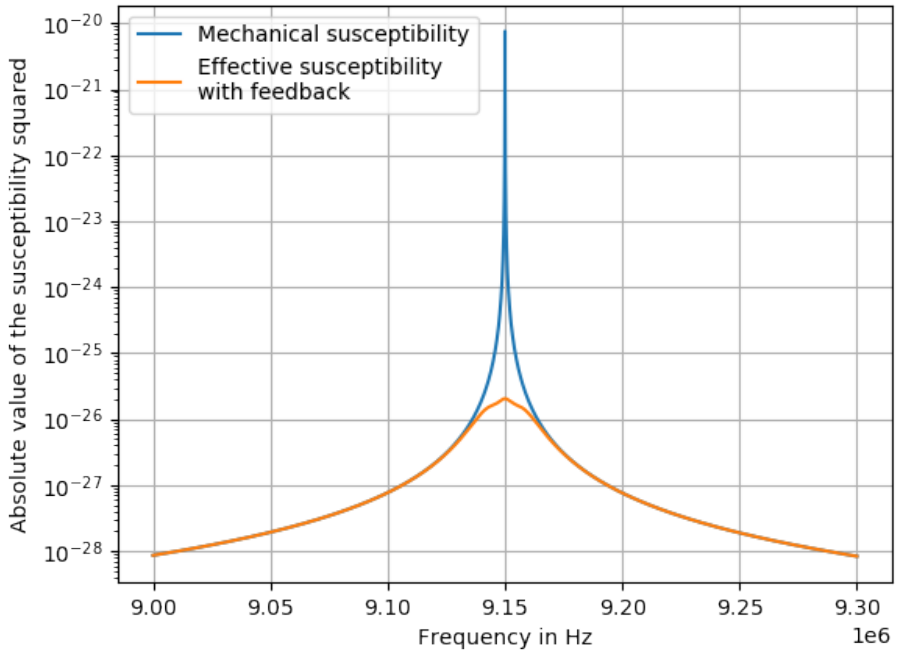

Figure 3.7: Simulated effective susceptibility with various values for parasitic feedback gain g_a. We can see that the self feedback nullifies the wanted feedback effect, effectively returning the effective susceptibility to the unmodified mechanical susceptibility.

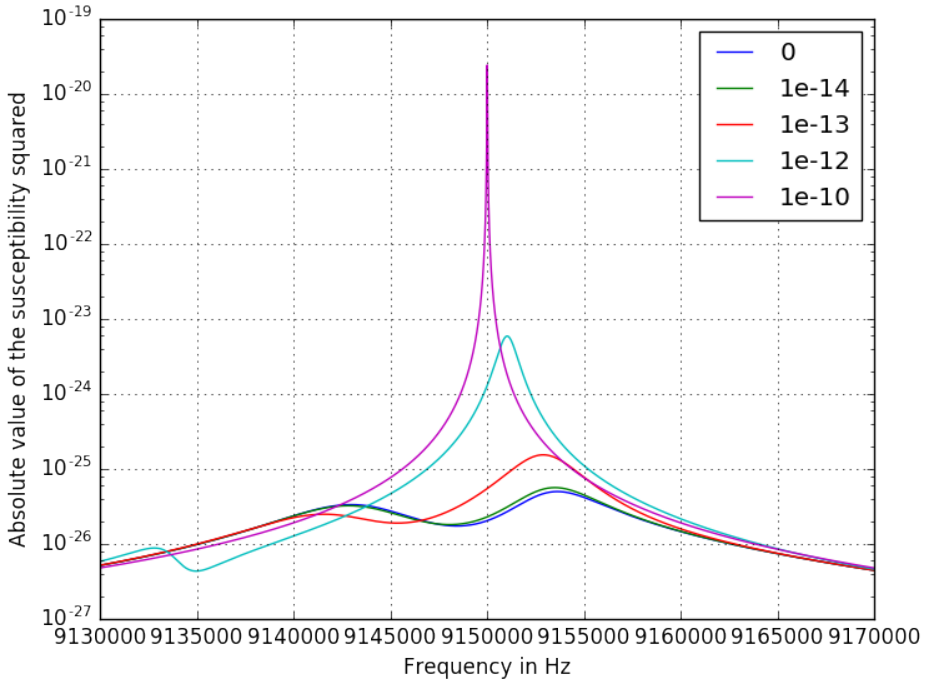

the previous equation and solving for y, we get

$$y = \frac{x + x_{imp}}{1 - ah_{fb}}.$$

From our block diagram 2.3 we find the expression for the feedback force $F_{fb} = h_{fb}y = h_{fb}(x + x_{imp} + z)$. We can see from the diagram that $z = aF_{fb}$, and solving for F_{fb} we get

$$F_{fb} = \frac{h_{fb}(x + x_{imp})}{1 - h_{fb}a}.$$

Now we can find the expression for the actual mechanical position x:

$$x = \chi_m(F_{tot} + F_{fb}) = \chi_m \left(F_{tot} + \frac{h_{fb}(x + x_{imp})}{1 - h_{fb}a} \right).$$

Again, solving for x, we get

$$x = \frac{\chi_m}{1 - \frac{\chi_m h_{fb}}{1 - h_{fb}a}} \left(F_{tot} + \frac{h_{fb}x_{imp}}{1 - h_{fb}a} \right).$$

From this we can see that for significant parasitic feedback, i.e. a large a, the oscillator real position approaches that of the no feedback case. Plugging this result back into the result for y, we finally get

$$y = \frac{\chi_m}{1 - ah_{fb} - \chi_m h_{fb}} \left(F_{tot} + \frac{h_{fb}x_{imp}}{1 - ah_{fb}} \right) + \frac{x_{imp}}{1 - ah_{fb}}.$$

The addition of the parasitic self-feedback changes the effective susceptibility to

$$\chi_{eff}(\Omega) = \frac{\chi_m(\Omega)}{1 - \frac{\chi_m(\Omega)h_{fb}(\Omega)}{1 - h_{fb}a}}.$$

With large a value, this converges onto just the plain mechanical susceptibility χ_m, while with a values approaching zero it converges to the effective susceptibility in absence of parasitic feedback, as expected.

Feedback cooling requires constant measurement of the phase quadrature. The measured quadrature is determined by the constant phase difference between the signal arm and the local oscillator arm of the homodyne measurement setup, which relates to the light path length difference between the arms. This path length is controlled by piezoelectric mirror, the position of which must be adjusted so that only the wanted quadrature

is measured. While doing the measurements, we failed to take this step due to our insufficient understanding of the underlying theory at the time. Instead, the piezo was set to sweep as in [20], in order to better find the optical resonance frequency for the cavity. This mistake further complicates the picture.

An attempt was made to get around this parasitic feedback problem by using a very narrow filter (a few hundred Hz bandwidth) in such a way, that only a portion of the signal line width gets captured by it. The idea was to then use the Red Pitaya iq modules to shift this narrow feedback signal by a small amount in frequency, such that the resulting feedback signal is outside of the bandpass, but still inside the mechanical linewidth. However, this approach did not get desired results, as the limited bandwidth meant very weak to nonexistent cooling performance. Furthermore, while the incoming and outgoing signals might have been separated in frequency by more than the bandpass bandwidth, because the bandpass filter is not a perfect square filter, there is still some room for parasitic feedback to happen with high gains.

4 Results and conclusions

Controller phase space was scanned through with various electronic gains and filter bandwidths. Any electronic gain on the Red Pitaya equal or larger than one resulted in self-feedback and saturation of the Red Pitaya output on some part of the controller phase space. The larger the bandwidth of the filter, the stronger the artifacting resulting from the parasitic feedback. Larger controller gains also resulted in larger portion of the phase space being affected, as can be seen in figure 4.1.

Fitting all the spectrums from the phase scan results (phase scans such as those in figure 4.1) into lorentzian functions, in order to get the fitting parameters of center frequency, area under the curve, and width at half-maximum (gamma), did not reveal any cooling effect, or much else of interest either. Cooling experiments were done in both 5K and 295K, and for two different samples. Plotting the fit parameters of gamma (width at half-maximum), center frequency and area, no meaningful trends can be found (see figure 4.2). The cooling effect, if it were there, would be visible in the flattening of the lorentzian fit of the measured mechanical spectrum at a certain controller phase (corresponding to the feedback phase being $\pi/2$ behind the mechanical phase), visible as an increase in the gamma fit parameter. There was no visible cooling even from room temperature, as can be seen in figure 4.3. The feedback experiments were done with various filter bandwidths. The effect of the bandwidth was that large bandwidths tended to amplify the instability and artifacting. There was some visible aliasing in the experiments with visible self-feedback, with artifacts exactly filter bandwidth apart from the filter center frequency. The fit results of the no-feedback case as a function of laser wavelength can be seen in figure 4.4. Here we can clearly see the phenomenon of optical spring effect, where driving the optical cavity out of resonance results in the shifting of the resonance frequency. The gamma, that is the mechanical dampening rate Γ_m can be seen from figure 4.4 to be roughly 3.5 ± 1kHz.

In an attempt to get around the self-feedback problem, shifting the feedback away from the bandpass filter range was tried (see figure 4.5). The idea was to have a narrow filter, capturing only part of the mechanical oscillation linewidth, and then shift the feedback signal to the other side

Figure 4.1: Practical effect of unwanted feedback on the homodyne detection. Here we can see the increasing parasitic feedback effect and artifacting with increasing controller gain. The filter bandwidth here is 77kHz. These measurements were performed in temperature of 5K, and all on the same occasion with the same sample.

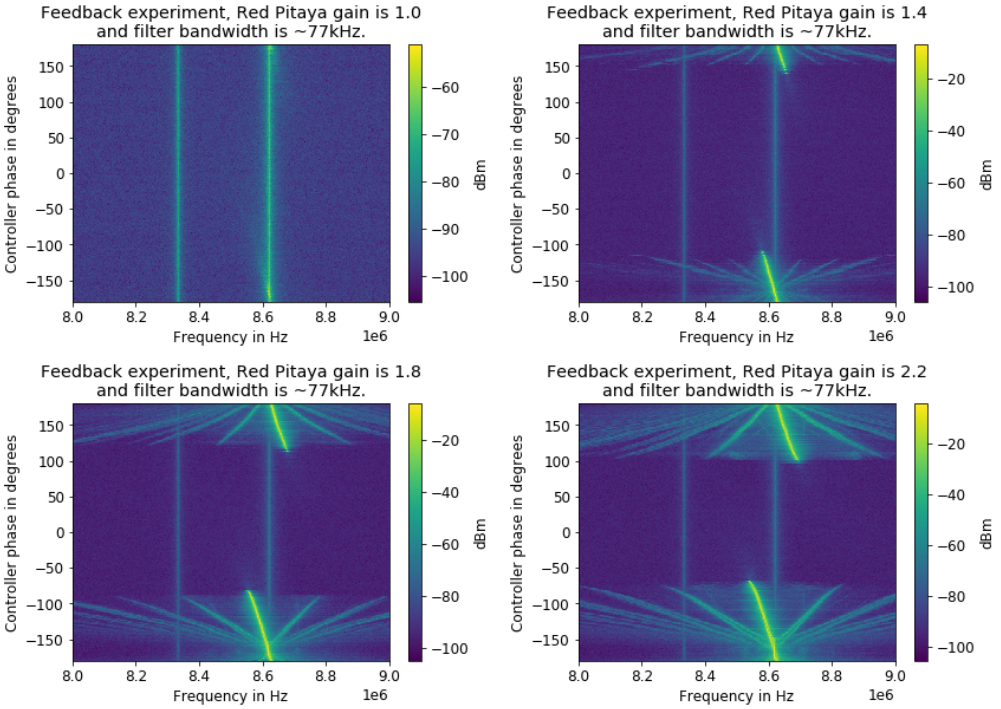

Figure 4.2: The measured spectrum while scanning through the controller phase, and the fitting parameters of lorentzian fits plotted against controller phase in degrees. Here the filter bandwidth is 7000Hz, and the electronic gain is 4. No meaningful trends can be found here, nor in any of the other fitted data from the feedback experiments. Due to strong artifacting interfering with the fitting, only the relatively "dark" part of the phase space data is fitted. The measurement was performed in 5K temperature.

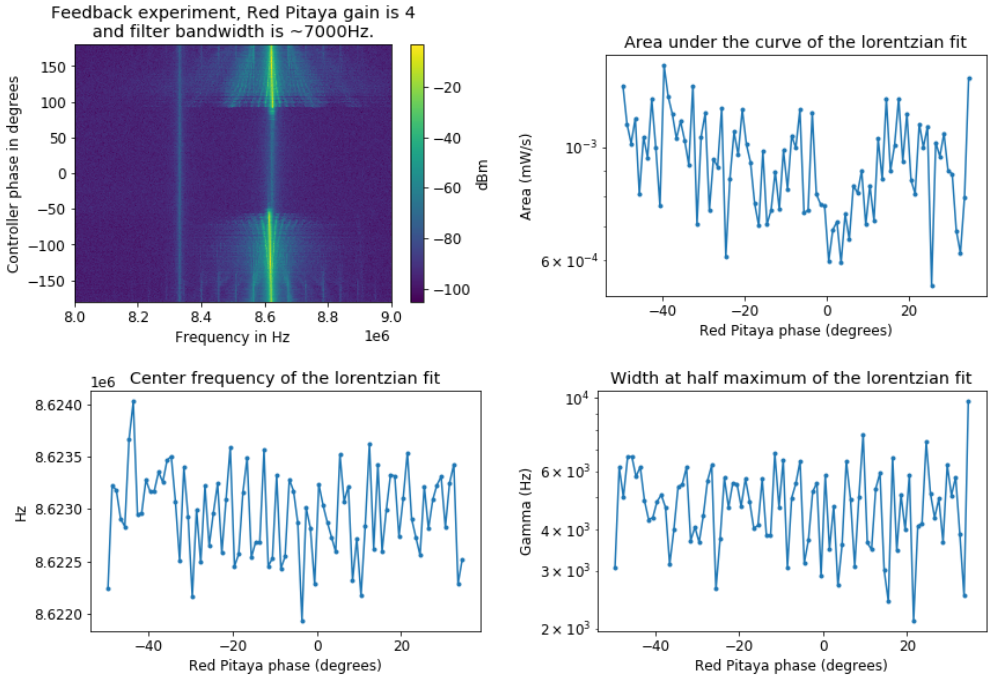

Figure 4.3: The measured spectrum while scanning through the controller phase, and the fitting parameters of lorentzian fits plotted against controller phase in degrees. Here the filter bandwidth is 1215Hz, and the electronic gain is 4. This experiment was done in room temperature (295K).

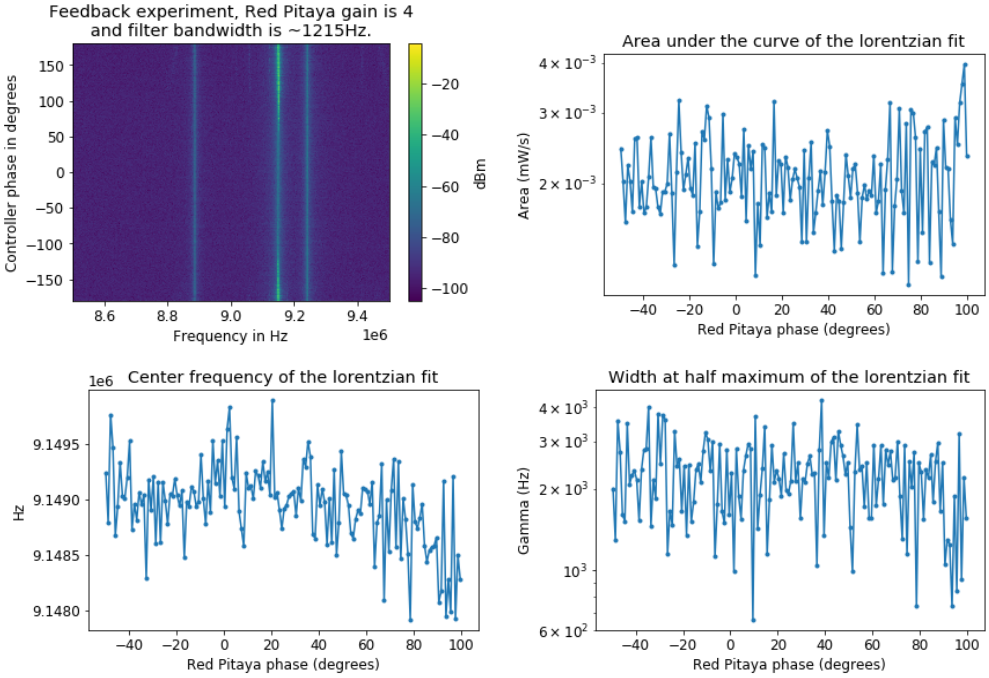

Figure 4.4: The spectrum scanning through the measuring laser wavelengths, and fitting parameters of lorentzian fits to the spectrum as a function of wavelength, in the case of no feedback. See the clear shift in cavity resonance frequency as a function of detuning, a.k.a. optical spring effect.

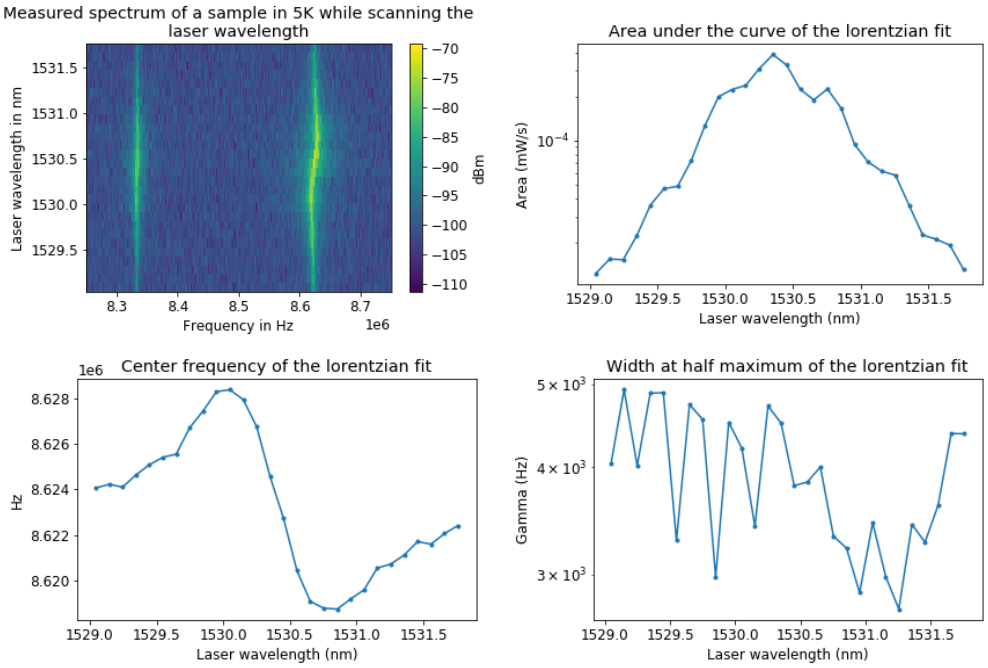

Figure 4.5: Feedback experiment with shifted feedback. Here the gain was 4, filter bandwidth was 303Hz and the feedback was shifted by 300Hz. No effect from the feedback can be seen here, parasitic or otherwise. The feedback shifting experiments were done on a different sample, hence the different peaks compared to figure 4.2.

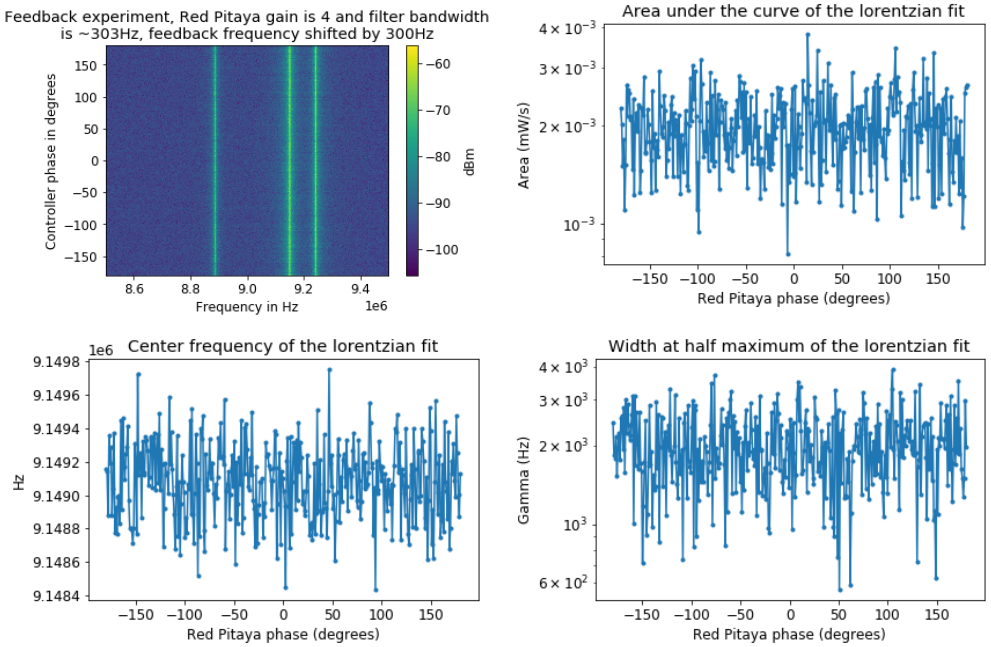

of the mechanical peak, away from the filter band. This way, the signal generated by the feedback would not get past the filter, thus eliminating the parasitic feedback. However, this approach was not effective, due to a few problems. Firstly, the center of the mechanical linewidth was not precisely measured, and thus the placement of the narrow bandpass filter was not optimal. Secondly, the narrowness of the filter meant that not all of the available information about the oscillator position was captured, thus reducing theoretical cooling performance. Thirdly, the bandpass filter implementation is not a perfect square filter, thus if the feedback signal was not shifted very far from the bandpass range, some of the feedback signal would still be picked up by the filter, although heavily attenuated, thus still causing some small amount of parasitic feedback. This approach was not analyzed theoretically.

Achieving feedback cooling while using the same laser for both measure-

ment and feedback should be possible if the EOM is moved to the signal branch, as this has been done in [25]. One simple way to get around the self-feedback problem is to use two lasers with orthogonal polarizations: one to continuosly measure the oscillator position and the other for the feedback loop (see [9]). Another way is to use an Acousto-Optic modulator (AOM) instead of an EOM, by splitting the beam and modulating only the other fork, while also shifting the frequency of the modulated beam[5].

The effect of the incorrect piezo settings was not analyzed here, and it is in principle possible that the parasitic feedback would not be strong enough to be a problem with correct piezo position. In the future, it might be worthwhile to first only correct the piezo position, and see if the parasitic feedback still behaves in the same way. Once the parasitic feedback problem has been mitigated in some way, the cooling performance should be primarily limited by the measurement efficiency.

In this work, the laser wavelength was set to cavity resonance manually, and not locked via feedback loop, as is usually done. This introduces another possible source of error, due to the nonzero detuning of the laser (see equation (2.4)). This souce of error was likely small compared to all the other problems with the experiment, but it should be eliminated in the future by properly locking the laser to the cavity resonance. This can be done, for example, with the Red Pitaya and the pyrpl lockbox module[24].

4.1 Summary and outlook

Feedback cooling of the split silicon beam photonic crystal structure was tried, but failed to produce measurable cooling because of several errors made during the setup of the experiments. Perhaps the largest of the errors was setting the piezo to sweep, instead of locking onto the correct homodyne phase to measure the phase-quadrature of the light scattered from the cavity (see equation (2.4)). Another error was positioning of the EOM before the split into the signal and local oscillator arms of the homodyne interferometer, leading to strong parasitic self-feedback (see figures 4.2 and 4.3) of the laser amplitude modulation. This parasitic feedback effect was analyzed by the use of control theory, but due to other compunding issues, such as the aforementioned incorrect piezo sweep, as well as the limited output of the Red Pitaya causing saturation effects with high self-feedback, no definite conclusions could be drawn from the analysis. Another compounding issue was that the laser was tuned to the cavity resonance manually, leading to some amount of detuning.

Looking forward, it seems likely that the issues encountered in this work with unwanted parasitic feedback can be overcome relatively easily, simply by correcting the errors meantioned previously. A very similar experiment has been done recently by Guo et al[25], where they managed to perform feedback cooling using only one laser for both measurement and feedback, the same way we tried to accomplish here. Since they did not report running into any trouble with self-feedback in this paper, it seems likely that the troubles we encountered were caused by the our mistakes, rather than any kind of fundamental limitation. The structure itself should be suitable for feedback cooling, being a "bad cavity". Once the problems with the experiment are corrected, the main factor limiting cooling performance will probably be the relatively large cavity losses inherent in our oscillator structure, leading to poor measurement efficiency η. The parameters of our oscillator likely preclude ground state cooling, but that was never our goal to begin with. Even though cooling was not achieved in this experiment, we learned a lot about the practicalities of feedback cooling, and are optimistic about future experiments using the same basic setup.

Bibliography

[1] T.W. Hänsch and A.L. Schawlow: Cooling of gases by laser radiation, Optics Communications Volume 13, p. 68-69, January 1975

[2] D.J. Wineland, R.E. Drullinger and F.L. Walls: Radiation pressure cooling of bound-resonant absorbers, Physical Review Letters Volume 40, Article Number 1639, 19.06.1978

[3] V. B. BRAGINSKII, A. B. MANUKIN, and M. Yu. TIKHONOV: Investigation of dissipative ponderomotive effects of electromagnetic radiation, Soviet Physics JETP, Volume 31, Number 5, p. 829-830, November 1970

[4] A. Dorsel et al: Optical Bistability and Mirror Confinement Induced by Radiation Pressure, Physical Review Letters Volume 51, Article Number 1550, 24.10.1983

[5] P. F. Cohadon, A. Heidmann, and M. Pinard: Cooling of a Mirror by Radiation Pressure, Physical Review Letters Volume 83, Number 3174, 18.10.1999

[6] Stefano Mancini, David Vitali, and Paolo Tombesi: Optomechanical Cooling of a Macroscopic Oscillator by Homodyne Feedback, Physical Review Letters Volume 80, Article Number 688, 1998

[7] M. Poggio, C.L. Degen, H.J. Mamin, and D. Rugar: Feedback Cooling of a Cantilever's Fundamental Mode below 5 mK, Physical Review Letters Volume 99, Article Number 017201, 02.07.2007

[8] A. Kubanek et al: Photon-by-photon feedback control of a single-atom trajectory, Nature Volume 462, p. 898–901, 2009

[9] Massimiliano Rossi, David Mason, Junxin Chen, Yeghishe Tsaturyan and Albert Schliesser: Measurement-based quantum control of mechanical motion, Nature Vol 563, p. 53-58, 1.11.2018

[10] H.M. Wiseman and G.J. Milburn: Quantum Theory of Optical Feedback via Homodyne Detection, Physical Review Letters Vol 70, Article Number 548, February 1993

[11] A. C. Doherty and K. Jacobs: Feedback control of quantum systems using continuous state estimation, Physical Review A Volume 60, Article Number 2700, October 1999

[12] Jing Zhang, Yu-xi Liu, Re-Bing Wu, Kurt Jacobs, and Franco Nori: Quantum feedback: Theory, experiments, and applications, Physics Reports Volume 679, p. 1-60, 27.03.2017

[13] Constanze Höhberger Metzger and Khaled Karrai: Cavity cooling of a microlever, Nature Vol 432, p.1002-1005, December 2004

[14] O. Arcizet, P.-F. Cohadon, T. Briant, M. Pinard, and A. Heidmann: Radiation-pressure cooling and optomechanical instability of a micromirror, Nature Vol 444, p. 71-74, November 2006

[15] A. Schliesser, Del'Haye, N. Nooshi, K. J. Vahala, and T. J. Kippenberg: Radiation Pressure Cooling of a Micromechanical Oscillator Using Dynamical Backaction, Physical Review Letters Volume 97, Article Number 243905, 2006

[16] R. W. Peterson, T. P. Purdy, N. S. Kampel, R. W. Andrews, P.-L. Yu, K. W. Lehnert, and C. A. Regal: Laser Cooling of a Micromechanical Membrane to the Quantum Backaction Limit, Physical Review Letters Volume 116, Article Number 063601, 2016

[17] Markus Aspelmeyer, Tobias J. Kippenberg and Florian Marquardt: Cavity Optomechanics, Reviews of Modern Physics Volume 86, Article Number 1391, December 2014

[18] Warvick P. Bowen and Gerard J. Milburn: Quantum Optomechanics, CRC Press Taylor & Francis Group, 2015

[19] C. Genes, D. Vitali, P. Tombesi, S. Gigan, and M. Aspelmeyer: Ground-state cooling of a micromechanical oscillator: Comparing cold damping and cavity-assisted cooling schemes, Physical Review A Volume 77, Article Number 033804, 2008

[20] Rick Leijssen, Giada R. La Gala, Lars Freisem, Juha T. Muhonen and Ewold Verhagen: Nonlinear cavity optomechanics with nanomechanical thermal fluctuations, Nature Communications Volume 8, Article Number 16024, 7.7.2017

[21] Christopher C. Gerry and Peter L. Knight: Introductory Quantum Optics, Cambridge University Press, 2004

[22] Apurva Singh Chauhan, A.Mukund Lal, Varun Maheshwari and D.Bhagwan Das: Hardware Implementation of DSP Filter on FPGAs, International Journal of Computer Applications, Volume 62, p. 34-37, January 2013

[23] The website for Red Pitaya (aka. STEMlab) `www.redpitaya.com`

[24] The website for the pyrpl software package: `https://pyrpl.readthedocs.io/en/latest/index.html`

[25] Jingkun Guo, Richard Norte, and Simon Gröblacher: Feedback cooling of a room temperature mechanical oscillator close to its motional groundstate, Physical Review Letters Volume 123, Article Number 223602, 27.11.2019